Progress in Additive Manufacturing (2023) 8:495–503
https://doi.org/10.1007/s40964-022-00340-4

FULL RESEARCH ARTICLE

L-PBF for the production of metallic phononic crystal: design and functional characterization

Francesco Rosa[1] · Gabriele Cazzulani[1] · Davide Enrico Quadrelli[1] · Riccardo Casati[1]

Received: 27 June 2021 / Accepted: 26 August 2022 / Published online: 9 September 2022
© The Author(s) 2022

Abstract
Vibration abatement often requires the adoption of peculiar solutions and/or foundations. This paper presents an innovative solution to this problem, consisting in a phononic meta-material realized via Laser Powder Bed Fusion (L-PBF) capable to prevent the propagation of vibrations within specific frequency ranges. The integration of this meta-material within existing supporting structures can, therefore, greatly reduce the needing of foundations capable to stop vibrations. After a description of the design procedure of the meta-material that shows how to satisfy the constraints imposed by L-PBF technology, the manufactured sample is described and analyzed to predict its band-gaps. Finally, the theoretical results are compared with experimental measurements. These results show a good agreement between expected and actual meta-material behavior.

Keywords Additive manufacturing (AM) · Laser Powder Bed Fusion (L-PBF) · Phononic crystals · Vibrations · Design · Lattice · Meta-materials

1 Introduction

Additive manufacturing (AM) allows for the production of components layer by layer, reducing the design constraints imposed by traditional manufacturing technologies. Its intrinsic higher flexibility enables the manufacturing of components and structures with very complex shapes that other technologies cannot realize, widening designers' possibilities and leading to a radical change in how parts are conceived, designed and embedded into final products [1–4]. Although the design freedom is wide, it is not unlimited [5, 6]. Different constraints characterize AM technologies, and a number of studies investigated such limits to derive adequate design strategies and guidelines [1, 2, 25]. Several AM technologies are currently used for producing metallic objects, including beam-based and non-beam-based methods [7]. However, only powder bed technologies, namely Laser Powder Bed Fusion (L-PBF), Electron Beam Melting and Binder Jetting, allow producing metal objects with very complex shape [8]. Each of these techniques have different constraints for part design. L-PBF is currently the most widely employed AM technology and it allows producing parts with several materials, including Fe, Ti, Al alloys [9].

One of the possibilities given by AM consists in the fabrication of periodic lattice structures offering peculiar functional and structural properties that can be exploited in several applications [10–12]. They are conceived as a 3D pattern of a unit cell specifically designed to avoid discontinuities. The overall properties of lattice structures mainly depend on the design of the unit cell, including geometry and material properties [13, 14]. Phononic crystals (PCs) are engineered periodic structures (meta-materials) able to control elastic wave propagation, since they exhibit Bragg-type stopbands due to the destructive interference between transmitted and reflected elastic waves at certain frequency ranges [15–17]. AM has been recently used for fabricating complex 3D PCs [18–20], but most of the research works focused on 3D printing of polymer PCs, while very few have been dedicated to the case of metallic lattices [21, 22]. However, metallic PCs can be very relevant for several applications since they can be potentially integrated in parts for

✉ Riccardo Casati
riccardo.casati@polimi.it

Francesco Rosa
francesco.rosa@polimi.it

Gabriele Cazzulani
gabriele.cazzulani@polimi.it

Davide Enrico Quadrelli
davideenrico.quadrelli@polimi.it

[1] Dip. di Meccanica, Politecnico di Milano, via La Masa, 1, Milan, Italy

structural applications, conferring tailored functional properties to mechanical systems, such as attenuation of vibration and reduction of noise.

Given this background, this work is aimed at investigating the possibility to exploit AM technologies for producing parts that embed metallic PCs able to provide control of vibrations. More in details, this paper, first, describes the design process of a PC unit cell, highlighting the effects of L-PBF manufacturing constraints in combination with cell size and on bandgap opening and closing frequencies. Using this cell, a *A357* aluminum alloy PC structure was designed, printed, analyzed by SEM to investigate the occurrence of defects and tested to characterize its dynamic response by laser vibrometer.

2 Design of the PC unit cell

PCs were produced by L-PBF, a very common AM technology that allows fabricating metal parts with complex shapes and small geometrical features. The possibility of embedding meta-materials within mechanical components and the constraints given by the size of the building chamber of conventional L-PBF limit the maximum dimensions of the unit cell. In this work the size of the unit cell was limited to 10 mm to ease the subsequent dynamic testing.

The dynamic response of a lattice cell, and thus the appearance of bandgaps in specific frequency regions, depends on the design parameters of the unit cell in terms of geometry, material and size. In this work, material and size were not changed, therefore the geometry was designed to tailor mass and stiffness distribution of the unit cell and consequently its frequency-dependent behavior. The design optimization of the unit cell started from the analysis of the very simple Body Centered Cubic (BCC) cell represented in Fig. 1a. The dispersion relation of this unit cell, determined with COMSOL Multi-Physics 5.4 and displayed in Fig. 1b, shows that the frequency range of the first complete bandgap of the BCC lattice is very high (above 700 kHz, corresponding to the frequency range with no solutions in Fig. 1b). This means that a standard unit cell cannot be used for vibration suppression purposes in typical frequency regions of interest for mechanical applications, but, to reduce the bandgap frequencies, to target mechanical applications, a proper design of the unit cell is necessary.

A qualitative relationship between natural frequency and dimensions of the cell was first derived by relying on the fact that this investigation is focused on mono-axial tests, thus the whole specimen can be roughly approximated to an axially loaded beam. The natural frequencies of such type of system are proportional to the square root of the ratio between equivalent elastic modulus (E^*) and equivalent density (ρ^*) of the structure itself. Thus, the following relationship can be derived:

$$\omega_n^* = \text{cost} \cdot \sqrt{\frac{E^*}{\rho^*}} = \text{cost} \cdot \sqrt{\text{cost} \cdot \frac{d^4}{a^4} \cdot \frac{d^2}{a^2}} = \text{cost} \cdot \left\| \frac{d}{a} \right\| = \text{cost} \cdot \frac{d}{a}, \tag{1}$$

where a is cell size and d is the beam section size. According to Pasini and Vigliotti [13] and Ashby [27], ρ^* and E^* were calculated as follows:

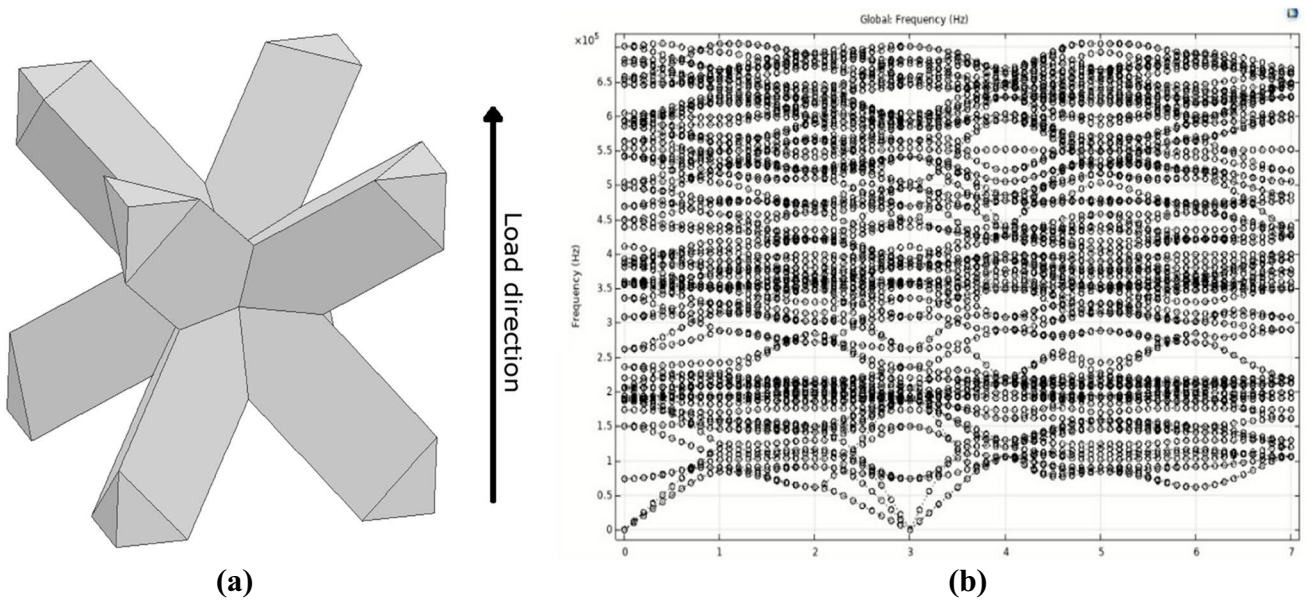

Fig. 1 Initial cell: standard BCC unit cell (**a**) and corresponding dispersion relation (**b**)

$$\rho^* = \text{cost} \cdot \frac{A}{a^2} = \text{cost} \cdot \frac{d^2}{a^2},$$
$$E^* = \text{cost} \cdot \frac{I}{a^4} = \text{cost} \cdot \frac{d^4}{a^4},$$

where A is beam cross-section area of the beam and I is the moment of inertia of beam cross section. Equation 1 shows that the first axial natural frequency of a lattice with the cell geometry depicted in Fig. 1 linearly increases with beam size, while it is inversely proportional with respect to cell size.

To reduce natural frequencies, according to Eq. 1, thinner beams were considered a mass was applied at the center of the unit cell. Figure 2 shows four embodiments of the modified BCC cell.

COMSOL Multiphysics 5.4 was used to simulate the cell dynamic response and to determine bandgaps opening and closing frequencies of the cells shown in Fig. 2. The simulation was performed considering the characteristics of the aluminum alloy ($E = 69$ GPa, $\rho = 2700$ kg/m^3, $\nu = 0.33$) and imposing the periodic boundary condition on the unit cell. The results of the simulations are listed in Table 1 and depicted in Fig. 3. As expected, bandgap opening frequency linearly increases with beam cross section size. To further confirm Eq. 1, three different cells were generated by scaling the Cell-1, by a factor of 0.5 (Cell-1F), 1.5 (Cell-1D) and 2.0 (Cell-1E). The diagram of Fig. 3 confirms the inverse proportional relationship between the bandgap opening and closing frequencies and the cell size.

The numerical analysis demonstrates that it is possible to design a BCC cell that have a band gap with opening and closing frequencies in the acoustic region, but also it also shows that such cell must have an additional mass at its

Table 1 Opening and closing band-gap frequencies with different strut dimensions

Cell name	d [mm]	ω_{open} [kHz]	ω_{close} [kHz]
Cell-1	2.76	96.50	122.17
Cell-1A	1.50	52.42	95.39
Cell-1B	1.20	42.23	81.43
Cell-1C	0.75	26.72	56.02

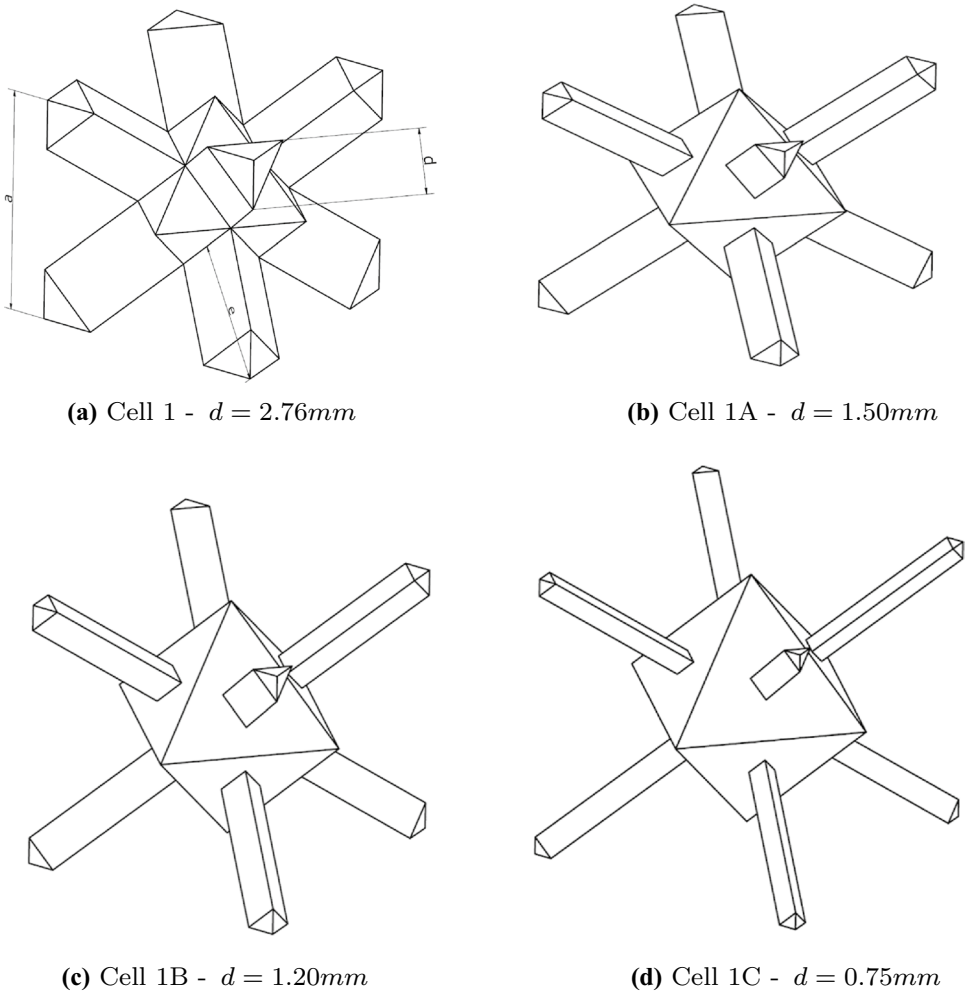

(a) Cell 1 - $d = 2.76mm$ **(b)** Cell 1A - $d = 1.50mm$

(c) Cell 1B - $d = 1.20mm$ **(d)** Cell 1C - $d = 0.75mm$

Fig. 2 Cells with different strut dimension and $a = 10$ mm

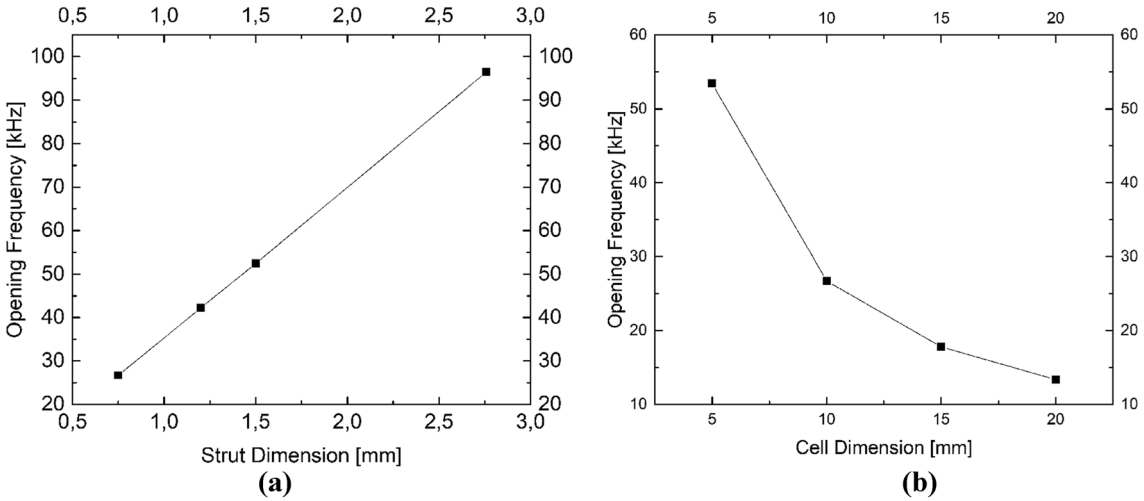

Fig. 3 Band-gap opening frequency as a function of strut dimension (**a**) and of cell size with $d = 2.76$ mm (**b**)

center and must be bigger than 10 mm, thus above the cell size limit set for this study. A further development of cell geometry was therefore necessary to achieve the target bandgaps. The cell design has also to respect limitations imposed by the AM system. Although the adoption of L-BPF reduces manufacturing constraints, some limitations persist. Many scholars have investigated on this topic and published several papers describing detailed design rules for AM [29]. In particular, it is important to consider that

1. support structures are needed for large overhang or inclined surfaces to dissipate efficiently the heat produced during metal powder melting;
2. the geometrical resolution of the process is closely related to the dimension of the melt pools, hence details smaller than the melt pool size cannot be manufactured.

Powder particles and sputters can also weld to the melt pool boundaries, affecting the final roughness and dimensional accuracy of parts. All these considerations greatly depend on the material, L-PBF system and process parameters. The inner part of a lattice structure is not accessible for support removal, thus the design constraints presented and discussed in [32–34] as well as the Renishaw AM250 capabilities provided by Renishaw itself were taken into account for the present work.

Considering these design guidelines and the results of simulations, two strategies were followed to design cells with reduced bandgap frequencies:

1. the mass at the center of the cell was increased,
2. curved beams with lower bending stiffness were introduced.

In particular, the section of the mass was increased gradually in the direction normal to the build direction in order to avoid overhangs larger than those allowed. The mass was built with surfaces inclined at 45° with respect to the build direction from four curved struts linked to the base of the cell. To reduce struts stiffness, their diameter was reduced to 0.6 mm and curved axis was adopted. Figure 4 shows the final design of the cell, while the full 3D step model of the cell, with all the detailed dimensions is attached as supplementary material.

COMSOL Multiphysics was then used to determine the dispersion relation of the final cell (Fig. 5. This diagram shows two bandgaps below 40 kHz: the first is between 16.6 and 28.6 kHz, the second is between 32.0 and 36.5 kHz.

3 Materials and experimental methods

Gas-atomized *A357* aluminum alloy powders with size distribution within the range of 20–63µm were employed to print the PC meta-material specimens used for the experiment with a Renishaw AM250 L-PBF system. The Renishaw AM250 installs a 200 W single-mode fiber laser with an estimated beam diameter at focal point of 75 µm. Laser melting is performed by discrete laser spots under argon atmosphere. The process parameters were set as follow:

- Hatch distance = 115 µm
- Point distance = 80 µm
- Exposure time = 140 µs
- Focal point = 1 mm above the powder bed
- Layer thickness = 25 µm
- Power = 200 W

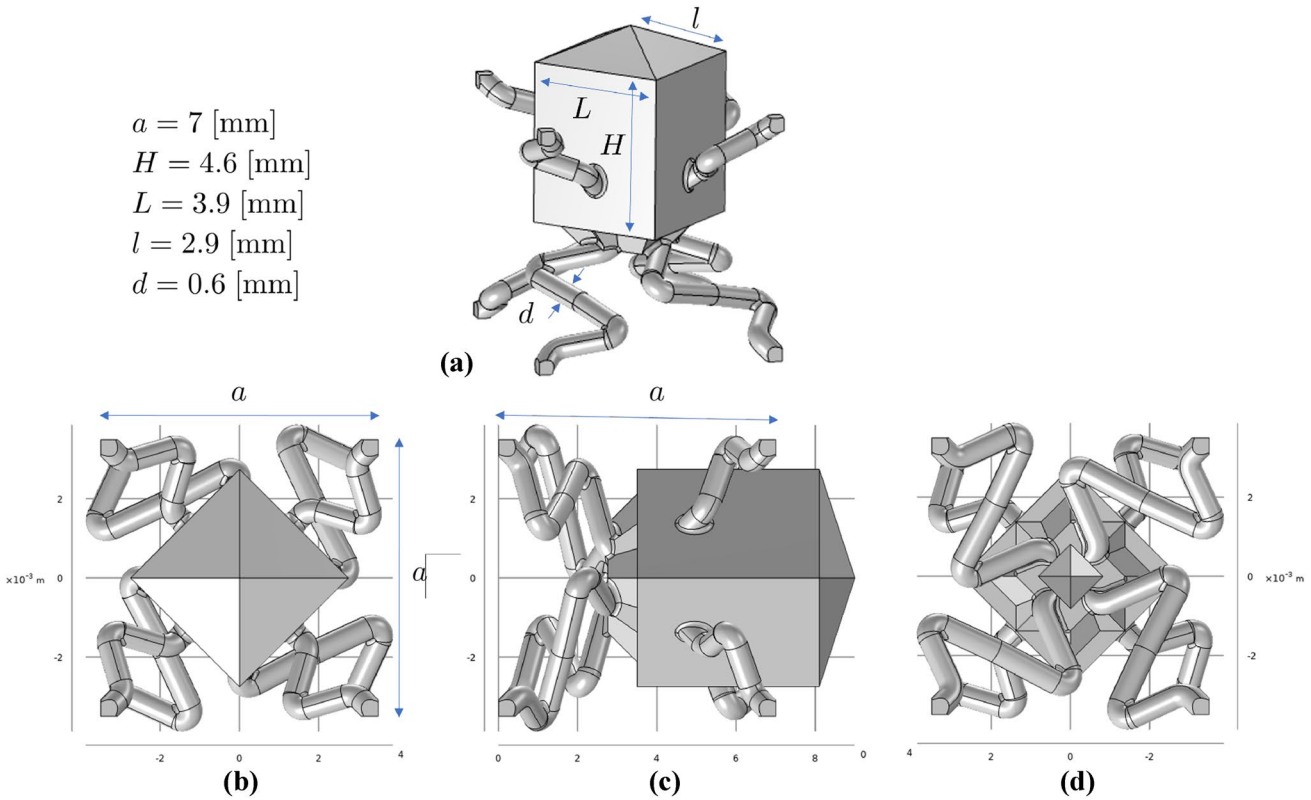

Fig. 4 Final cell: 3D (**a**), top (**b**), lateral (**c**) and bottom (**d**) view of the unit cell. The printing direction is from bottom to top of (**a**)

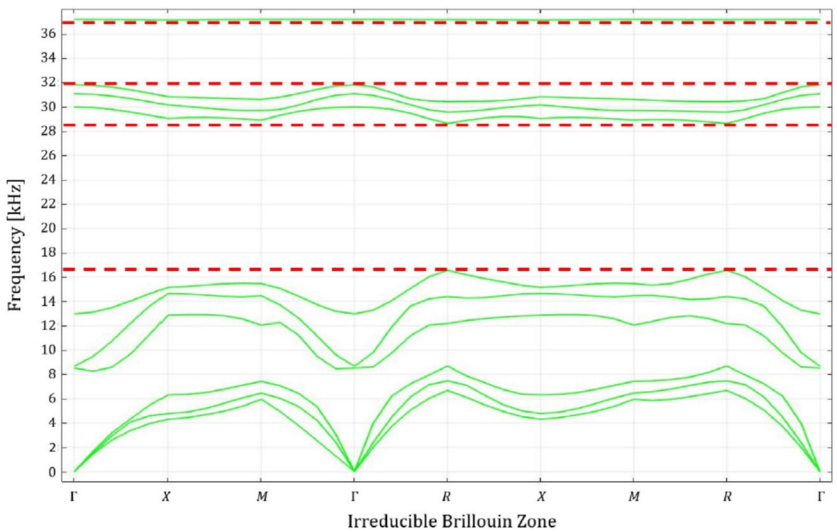

Fig. 5 Dispersion relation of the cell showed in Fig. 4

– Meander scanning strategy (scanning direction was rotated by 67° after each layer completion)

Figure 6 shows the manufactured PCs meta-materials made up by $3 \times 3 \times 9$ cells with geometry shown in Fig. 5. Two plates were added to fix the object on the testing rig. Surface analysis of the printed part was carried out by Zeiss EVO 50 scanning electron microscope (SEM).

The dynamic analysis was performed by constraining the lattice structure to a rigid aluminum block, where an inertial excitation shaker was placed (see 7) to make the block vibrate and transmit the excitation to the specimen. The

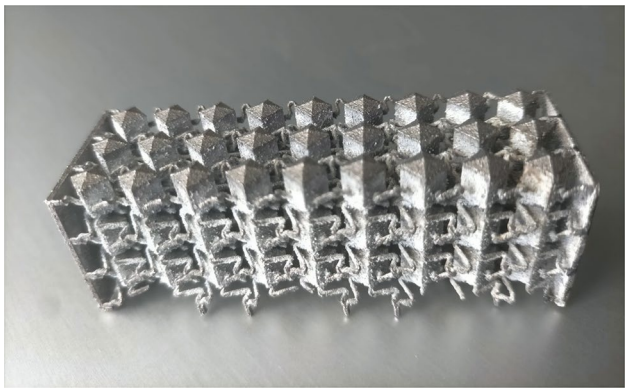

Fig. 6 manufactured PC meta-material

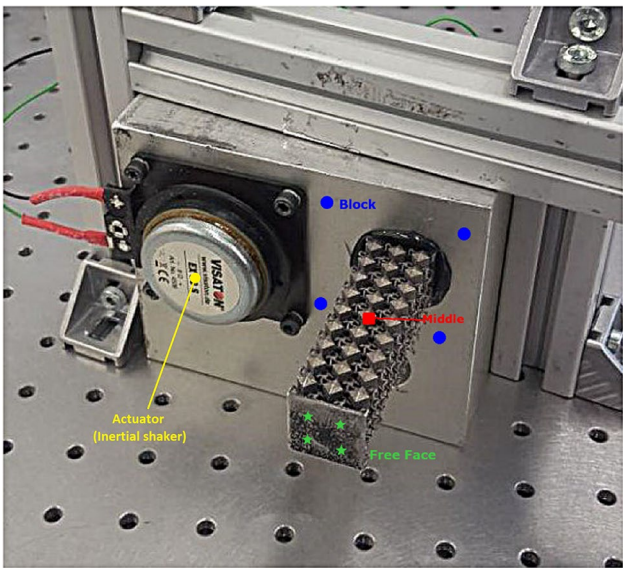

Fig. 7 Measurement scheme for the vibrometer tests

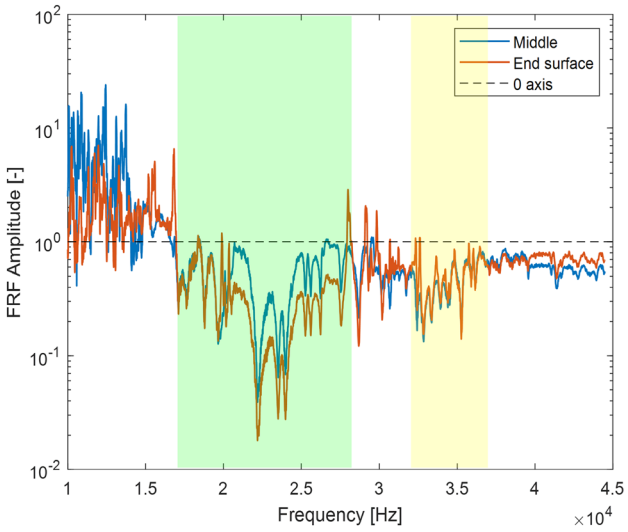

Fig. 8 FRF between the base vibration and the free face vibration of the specimen

actuator was properly selected to allow the excitation of the lattice structure in the interested range of frequencies and to provide low excitation forces avoiding possible plasticization of the lattice. The system was placed on an anti-vibration table to filter out all the possible vibration sources coming from the environment.

The lattice vibration was measured by means of a 3D laser scanning vibrometer (Polytec PSV-500-3D-H). The velocity of different points was measured on the lattice and on its constraint (Fig. 8), guaranteeing the synchronization of the different tests through a proper triggering system. As shown in Fig. 7, the vibrations in different points have been measured:

– Block (blue round marks): the aim of these measurements is to quantify the vibration velocity input provided to the lattice by its ground constraint. Four points were acquired at the four corners of the lattice to provide the average input in the longitudinal direction of the lattice itself;
– Free face (starred green marks): the aim is to identify the transfer function between the block (input) and free face (output) of the lattice, focusing in particular on longitudinal waves. In other words, this measurement provides the information about the vibration reduction inside the bandgaps along the lattice structure. As for the block, four measurements were acquired nearby the four corners of the free face;
– Intermediate point (square red mark): one measurement was collected at the mid length of the lattice to verify the progressive reduction of vibrations along the structure inside the bandgaps.

4 Results and discussion

Dynamic tests have been carried out to investigate the frequency range of the lattice bandgaps.

The test was done providing a sweep-sine input to the inertial actuator, so that the whole frequency range of interest could be analyzed at one time. The same result could have been obtained theoretically with a random input, but sweep sine provides a higher energy content in the desired frequency range, and thus a better signal-to-noise ratio of the output signals.

Figure 9 shows on a logarithmic scale the *Frequency Response Function* (FRF) between the vibrations of the block and those of two points along the specimen (the free face and the middle point of the specimen, corresponding to the 5th cell) along the longitudinal direction

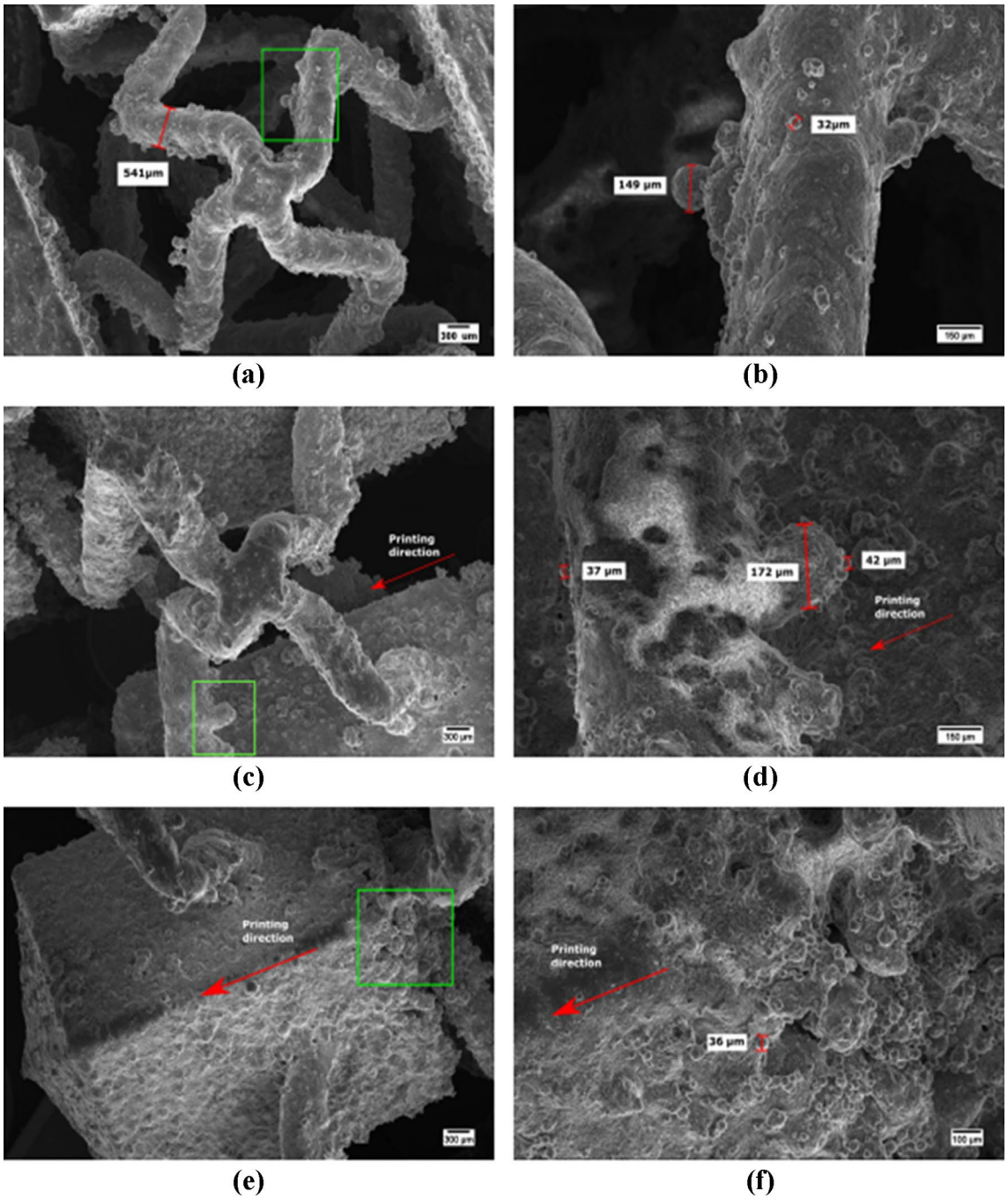

Fig. 9 FRF between the base vibration and the free face vibration of the specimen

of the specimen. A value lower than zero corresponds to vibration attenuation along the specimen. The colored rectangles correspond to the theoretical location of the first (green) and second (yellow) bandgap. The first bandgap is clearly visible in the frequency range between 16.5 and 28.5 kHz, coherently with the result expected from the dispersion relation. As expected, the vibration attenuation inside the bandgap increases along the structure, making the FRF amplitude at the end point lower than that at the middle point. Some resonance peaks, due to local effects produced by the finite boundaries of the structure, are present inside the bandgap itself. It is possible also to notice that for increasing frequencies the vibration reduction due to bandgaps is reduced, and the second bandgap, even if still visible in the expected range, results in a lower vibration attenuation. A possible explanation of this

phenomenon is related to the increased damping effect for increasing frequencies. At frequencies outside the bandgaps (white-background parts of the figure) many peaks are visible in the FRF due to the specimen resonances. Also this effect is reduced for increasing frequencies due to damping.

The prediction of the dynamic behavior of the lattice was made considering an ideal linear model, where all the beams of the lattice structure have constant thickness, no roughness or material discontinuities. Hence, small gap in the behavior of the physical and the simulated structure can be attributed to the presence of surface and bulk defects typical of this manufacturing process. Figure 9 show SEM images of the phononic crystal produced by L-PBF. Several particles with different size are welded to the surface. The size of some of these particles is in the range of PSD of the powder of the bed, other particles are coarser (e.g. 149 µm, 172 µm in the Fig. 9), therefore they are sputters ejected from the melt pool that are partially engulfed in the laser tracks. The presence of such particles makes the diameter of the beams inhomogeneous along their axis. Moreover, the average beam diameter (without considering the particles welded onto the surface) is slightly smaller than that designed, 540 µm vs 600 µm. However, the global behavior of the lattice seems not to be significantly affected by the mentioned defects and by the slight reduction of beam diameter, since the attenuation frequency range remains coherent with the bandgaps calculated for the nominal structure.

5 Conclusions

This paper focused on the design and the realization of a 3D lattice structure for vibration isolation made through metallic additive manufacturing. In particular, the phononic crystal structure has been designed and optimized to comply the manufacturing constraints of Laser Powder Bed Fusion and, at the same time, to provide a wide-band vibration attenuation within industrially relevant frequency ranges. Although the bandgap frequency range of the produced specimen is at the higher limit of the acoustic range, lower-frequency bangaps can be obtained with the same technology by increasing the cell size and consequently reducing its stiffness to mass ratio.

Dynamic tests were performed to investigate the frequency range of the lattice bandgaps. The first bandgap is noticeable between 16.5 and 28.5 kHz, in good agreement with the result expected from the dispersion relation. Moreover, as expected, the vibration attenuation increases along the structure. Slight differences in the behavior of the physical and the simulated structure were attributed to the presence of surface and bulk defects typical of LPBF process.

Acknowledgements Acknowledgements have been removed to make the paper anonymous.

Funding Open access funding provided by Politecnico di Milano within the CRUI-CARE Agreement.

Declarations

Competing interests The authors declare that they have no conflict of interest.

Open Access This article is licensed under a Creative Commons Attribution 4.0 International License, which permits use, sharing, adaptation, distribution and reproduction in any medium or format, as long as you give appropriate credit to the original author(s) and the source, provide a link to the Creative Commons licence, and indicate if changes were made. The images or other third party material in this article are included in the article's Creative Commons licence, unless indicated otherwise in a credit line to the material. If material is not included in the article's Creative Commons licence and your intended use is not permitted by statutory regulation or exceeds the permitted use, you will need to obtain permission directly from the copyright holder. To view a copy of this licence, visit http://creativecommons.org/licenses/by/4.0/.

References

1. Hague R, Campbell I, Dickens P (2003) Implications on design of rapid manufacturing. J Mech Eng Sci 217(25):25–30
2. Hague R, Mansour S, Saleh N (2004) Material and design considerations for rapid manufacturing. Int J Prod Res 42(22):4691–4708
3. ISO/ASTM 52910:2018(E) Additive manufacturing—design—requirements, guidelines and recommendations
4. Thompson MK, Moroni G, Vaneker T, Fadeld G, Campbell RI, Gibson I, Bernard A, Schulz J, Graf P, Ahuja B, Martina F (2016) Design for additive manufacturing: trends, opportunities, considerations, and constraints. CIRP Ann 65(2):737–760
5. Adam GAO, Zimmer D (2014) Design for additive manufacturing-element transitions and aggregated structures. CIRP J Manuf Sci Technol 7:20–28
6. Adam GAO, Zimmer D, Müller M (2014) Extension of prior developed design rules' range of validity for different boundary conditions in laser sintering, 2014. In: American Society for Precision Engineering, Proceedings of the ASPE—Spring Topical Meeting— dimensional accuracy and surface finish in additive manufacturing 57:30–35
7. ISO/ASTM 52900 (2015) Additive manufacturing general principles—terminology—ISO/ASTM 52900:2015 (E)
8. Zhang J, Jung Y-G (2018) Additive manufacturing: materials. processes, quantifications and applications. Butterworth-Heinemann (Imprint of Elsevier)
9. Thompson MK, Moroni G, Vaneker T, Fadel G, Campbell RI, Gibson I, Bernard A, Schulz J, Graf P, Ahuja B, Martina F (2016) Design for additive manufacturing: trends, opportunities, considerations, and constraints. CIRP Ann Manuf Technol 65:737–760. https://doi.org/10.1016/j.cirp.2016.05.004
10. Nguyen CHP, Kim Y, Choi Y (2019) Design for additive manufacturing of functionally graded lattice structures: a design method with process induced anisotropy consideration. Int J Precis Eng Manuf-Green Technol. https://doi.org/10.1007/s40684-019-00173-7

11. Tao W, Leu M (2016) Design of lattice structure for additive manufacturing. In: International Symposium on Flexible Automation (ISFA), pp 325–332
12. Kumar A, Collini L, Daurel A, YwanJeng J-Y (2020) Design and additive manufacturing of closed cells from supportless lattice structure. Addit Manuf 33:101168
13. Vigliotti A, Pasini D (2013) Mechanical properties of hierarchical lattices. Mech Mater 62:32–43. https://doi.org/10.1016/j.mechmat.2013.03.003
14. Ma F, Wang C, Liu C, Wu JH (2021) Structural designs, principles, and applications of thin-walled membrane and plate-type acoustic/elastic metamaterials. J Appl Phys 129:231103
15. Carta G, Brun M (2015) Bloch-Floquet waves in flexural systems with continuous and discrete elements. Mech Mater 87:11–26
16. Olhoff N, Niu B, Cheng G (2012) Optimum design of band-gap beam structure. Int J Solids Struct 49(22):3158–3169
17. Bertoldi K, Vitelli V, Christensen J, Van Hecke M (2017) Flexible mechanical metamaterial. Nat Rev Mater 2:17066
18. Elmadih W, Syam WP, Maskery I, Chronopoulos D, Leach R (2019) Multidimensional phononic bandgaps in three-dimensional lattices for additive manufacturing. Materials 12:1878. https://doi.org/10.3390/ma12111878
19. Waiel E, Syam Wahyudin P, Ian M, Dimitrios C, Richard L (2019) Mechanical vibration bandgaps in surface-based lattices. Addit Manuf 421–25:421–429. https://doi.org/10.1016/j.addma.2018.11.011 (**ISSN 2214-8604**)
20. Lucklum F (2018) Vellekoop MJ Bandgap engineering of three-dimensional phononic crystals in a simple cubic lattice. Appl Phys Lett 113(20):10. https://doi.org/10.1063/1.5049663
21. Wormser M, Wein F, Stingl M, Körner C (2017) Design and additive manufacturing of 3D phononic band gap structures based on gradient based optimization. Materials 10:1–15
22. Warmuth F, Wormser M, Köner C (2017) Single phase 3D phononic band gap material. Sci Rep 7:3843
23. Rosa F, Manzoni S, Casati R (2018) Damping behavior of 316L lattice structures produced by Selective Laser Melting, 15 December 2018, 160: 1010–1018
24. Lei H, Chuanlei L, Jinxin M, Hao Z, Yabo L, Xiaoyu Z, Panding W, Daining F (2019) Evaluation of compressive properties of SLM-fabricated multi-layer lattice structures by experimental test and μ-CT-based finite element analysis. Mater Des 169(5):107685
25. Thomas D (2009) The Development of Design Rules for Selective Laser Melting, Ph.D. Thesis, University of Wales Institute, Cardiff
26. Wohler Associates, Wohlers Report 2019, ISBN 978-0-9913332-5-7
27. Ashby MF (2006) The properties of foams and lattices. Phil Trans R Soc A 364:15–30. https://doi.org/10.1098/rsta.2005.1678
28. Adam GAO, Zimmer D (2014) Design for additive manufacturing-element transitions and aggregated structures. CIRP J Manuf Sci Technol 7:20–28
29. Adam GAO, Zimmer D, Müller M (2014) Extension of prior developed design rules' range of validity for different boundary conditions in laser sintering, 2014. In: American Society for Precision Engineering, Proceedings of the ASPE—SPRING TOPICAL MEETING—dimensional accuracy and surface finish in additive manufacturing 57:30–35
30. Choi M, Oh M, Koo B et al (2019) Optimal design of lattice structures for controllable extremal band gaps. Sci Rep 9:9976. https://doi.org/10.1038/s41598-019-46089-9
31. Müller B, Schnabel T, Oettel M, Töppel T, Gebauer M, Klöden B,Aumund-Kopp C, Hoschke K, Pfaff A (2017) Design for additive manufacturing. Guidelines and case studiesfor metal applications. CMTS 2017, Canadian Manufacturing Technology Show, Toronto, 25-28 September 2017
32. Calignano F (2014) Design optimization of supports for overhanging structures in aluminum and titanium alloys by selective laser melting. Mater Des 64:203–213
33. ISO/ASTM 52911-1:2019(E) Additive manufacturing—design—part 1: laser-based powder bed fusion of metal
34. ASTM F3413 (2019) Guide for additive manufacturing—design—direct energy deposition
35. Scalmana G (2019) Study on a SLM 3D printed lattice structure for vibration attenuation. MSc Thesis, Politecnico di Milano, Academic Year 2018/2019

Publisher's Note Springer Nature remains neutral with regard to jurisdictional claims in published maps and institutional affiliations.